

On Uncertainty Quantification in Particle Accelerator Modelling

Andreas Adelmann^a

^aPSI, Switzerland

Abstract

Using a cyclotron based model problem, we demonstrate for the first time the applicability and usefulness of an uncertainty quantification (UQ) approach in order to construct surrogate models. These surrogate model quantities for example emittance, energy spread, the halo parameter, and can be used to construct a global sensitivity model along with error propagation and error analysis. The model problem is chosen such that it represents a template for general high intensity particle accelerator modelling tasks. The presented physics problem has to be seen as hypothetical, with the aim at demonstrating the usefulness and applicability of the presented UQ approach and not solving a particular problem.

The proposed UQ approach is based on polynomial chaos expansions and relies on a *small* number of high fidelity particle accelerator simulations. Important uncertainty sources are identified using Sobol' indices within the global sensitivity analysis.

Keywords: Particle Accelerators, Uncertainty quantification; Polynomial chaos expansion; Global sensitivity analysis

1. INTRODUCTION

Uncertainty Quantification (UQ) describes the *origin*, *propagation*, and *interplay* of different sources of uncertainties in the analysis and behavioural prediction of generally complex and high dimensional systems, such as particle accelerators. With uncertainty, one might question how accurately a mathematical model can describe the true physics and what impact

Email address: andreas.adelmann@psi.ch (Andreas Adelmann)

the model uncertainty (structural or parametric) has on the outputs from the model. Given a mathematical model, we need to estimate the error. “How accurately is a specified output approximated by a given numerical method”? Can the error in the numerical solutions and the specified outputs be reliably estimated and controlled by adapting resources? For example, in beam dynamics simulations with space charge, grid sizes would be such a resource.

UQ techniques allow one to quantify output variability in the presence of uncertainty. These techniques can generally tackle all sources of uncertainties, including structural ones. However, in this paper we focus on parametric uncertainty of input parameters. The moments of the output distributions are sampled using Monte Carlo [1] or Quasi-Monte Carlo [2] methods, or newer approaches such as and Multi-Level Monte Carlo [3]. Other approaches exist and are known as non-sampling based methods. For an introduction to response surface methods see [4, 5]. The most popular method these days, which is used in this paper, is the Polynomial Chaos (PC) based method [6]. Strictly speaking, PC also requires sampling, but it is not random sampling as in Monte-Carlo type approaches.

Polynomial Chaos (PC) based techniques for propagating uncertainty and model reduction have been used in the past in almost all important scientific areas. An incomplete list consists of: climate modelling [7], transport in heterogeneous media [8], Ising models [9], combustion [10], fluid flow [11, 12], materials models [13], battery design [14], and Hamiltonian systems [15].

In probabilistic UQ approaches, one represents uncertain model parameters as random variables or processes. Among these methods, stochastic spectral methods [16, 17] based on polynomial chaos (PC) expansions [6, 18] have received special attention due to their advantages over traditional UQ techniques. For a more detailed discussion on that subject, consult the introduction of Hadigol et.al. [14], or alternatively, the book of Smith [19].

In the field of particle accelerator science, non-intrusive methods are far more attractive than intrusive methods. The complexity of the physics model would most likely require a total rewrite of the existing simulation packages, in order to facilitate intrusive methods. Because non-intrusive methods allow the use of existing beam dynamics codes as black boxes, they are the method of choice. In this paper, we use OPAL as the black-box solver. As we will see later, only independent solution realisations are

needed, hence embarrassingly parallel implementation is straightforward.

The proposed PC approach, first introduced in [16, 20], compute the statistics for Quantity of Interest (QoI) with a small number of accelerator simulations. However in contrast to [16, 20] we do not exploit the sparsity of expansion coefficients, this is subject to further research. Additionally, the presented UQ framework enables one to perform a global sensitivity analysis (SA) to identify the most important uncertain parameters affecting the variability of the output quantities.

To avoid confusion, we firstly point out a misnomer by mentioning that polynomial chaos [6] and chaos theory [21] are unrelated areas. Originally proposed by Norbert Wiener [6] in 1938 (prior to the development of chaos theory—hence the unfortunate usage of the term *chaos*), polynomial chaos expansions are a popular method for propagating uncertainty through low dimensional systems with smooth dynamics.

This work presents a sampling-based PC approach to study the effects of uncertainty in various model parameters of accelerators. As a model problem, we use the central region of a “PSI Injector 2 like” high intensity cyclotron. This paper’s focus is mainly to introduce UQ to the field of particle accelerator science and not to solve a particular problem. Without losing generality, we only consider the first 10 turns of the cyclotron.

In Section 2 we present our stochastic modelling approach which is based on non-intrusive PC expansions. After the derivation of the surrogate model, we then continue with reviewing a global sensitivity analysis approach using Sobol’ indices. Section 3 introduces the simulation model and the model problem. Section 4 applies the UQ to the stated problem, and shows the main features of this approach. The features are general in nature and *not* restricted to cyclotrons. Conclusions will be presented in Section 5.

2. UQ VIA POLYNOMIAL CHAOS EXPANSION

Wiener in 1938 [6] introduced polynomial chaos expansion. In 1991, Ghanem and Spanos [16] reintroduced this technique to the field of engineering. They first studied problems with Gaussian input uncertainties and extended their method to non-Gaussian random inputs. In their studies, orthogonal polynomials of the Askey scheme were used. This is known as a generalised polynomial chaos (gPC) expansion [20]. The method of gPC

expansion provides a framework to approximate the solution of a stochastic system by projecting it onto a basis of polynomials of the random inputs.

An overview and some details on the correspondence between distributions and polynomials can be found in [22]. A framework to generate polynomials for arbitrary distributions has been developed in [23]. The advantage of using polynomial chaos is that it provides exponential convergence for smooth models. However, the approach suffers from the curse of dimensionality, making them challenging for problems with number of parameters in the range $10 \dots 50$. To mitigate the curse of dimensionality, sparse grid techniques have traditionally been used [24, 25]. More recently, iterative methods to propagate uncertainty in complex networks have also been developed [26, 27, 28].

2.1. The surrogate model

Suppose you are designing or optimising complex particle accelerators. As a particular example, consider the case of a high intensity hadron machine. In such a machine one needs to characterise and minimise halo, and at the same time increase the beam quality, as one of the main design goals. Needless to say that this is a very simplistic picture, and other variables such as extracted energy, energy spread must also be considered. In order to accomplish this task, usually a large number of design parameters, in the search space \mathbf{D} (c.f. Figure 1), have to be considered.

In an ideal world you would run a number of high fidelity simulations (in some proportion to the size of \mathbf{D}) to solve the problem. However, even with state-of-the art tools in cases of practical interest, it is impossible to accomplish this task due to the prohibitive time to solution.

With the help of the surrogate model, there are 2 ways to tackle the problem. The first is to solve the problem approximatively on a coarser search space (red grid in Figure 1) and then "interpolate" to the true solution from the cheap to run surrogate model. The second option is to use the expensive high fidelity model to obtain $\mathbf{u}^* \in \mathbf{D}^*$, but on a much smaller domain (\mathbf{D}^*). It is important to mention that the surrogate model does not really reduce the search space. Rather, it is an approximation to the full model over the area of the search space where one believes that the model matters the most. The goal of the surrogate model is to create a cheap to sample approximation of the full model.

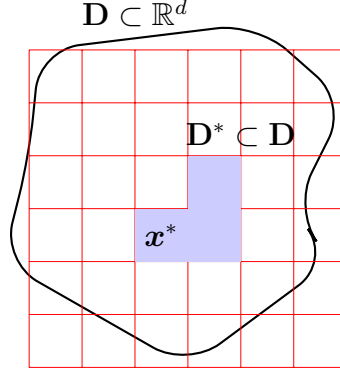


Figure 1: Design parameter search space \mathbf{D} , and one of the many possible configurations \mathbf{x}^* of the accelerator, leading to a desirable solution (working point). The red grid is depicting the training points, from which the surrogate model will be constructed. The equidistance of these points is not necessary, however it is sufficient to introduce the overall concept.

2.2. Mathematical bases of UQ

We briefly introduce the mathematical bases in the style and the notation of [19, 16, 20, 17, 14]. Let $(\Omega, \mathcal{F}, \mathcal{P})$ be a complete probability space, where Ω is the sample set and \mathcal{P} is a probability measure on \mathcal{F} , the σ -field (algebra) or Borel measure. Input uncertainties of the system has been discretised and approximated by the random vector $\boldsymbol{\xi} = (\xi_1, \dots, \xi_d) : \Omega \rightarrow \mathbb{R}^d$, $d \in \mathbb{N}$. The probability density function (pdf) of the random variable, ξ_k , is denoted by $\rho(\xi_k)$. Similarly, $\rho(\boldsymbol{\xi})$ represents the joint pdf of $\boldsymbol{\xi}$.

Let \mathbf{i} be a multi-index $\mathbf{i} = (i_1, \dots, i_d) \in \mathcal{I}_{d,p}$ and the set of multi-indices $\mathcal{I}_{d,p}$ is defined by

$$\mathcal{I}_{d,p} = \{\mathbf{i} = (i_1, \dots, i_d) \in \mathbb{N}_0^d : \|\mathbf{i}\|_1 \leq p\}, \quad (1)$$

where $\|\cdot\|_1$ is the l_1 norm i.e., $\|\cdot\|_1 = i_1 + \dots + i_d$, and p is the polynomial order.

All square integrable, second-order random processes with finite variance output, $u(\boldsymbol{\xi}) \in L_2(\Omega, \mathcal{F}, \mathcal{P})$, can be written as

$$u(\boldsymbol{\xi}) = \sum_{|\mathbf{i}|=0}^{\infty} \alpha_{\mathbf{i}} \Psi_{\mathbf{i}}(\boldsymbol{\xi}). \quad (2)$$

Hence α_i denotes the deterministic coefficients and $\Psi_i(\boldsymbol{\xi})$ are the multi-variate PC basis functions [19, 10.1.1] [16]. Note that the uncertain QoI, u , is represented by a vector of deterministic parameters α_i .

For the truncated PC Expansion (PCE) to order p in d dimensions of (2) we get

$$\hat{u}(\boldsymbol{\xi}) = \sum_{i \in \mathcal{I}_{d,p}} \alpha_i \Psi_i(\boldsymbol{\xi}). \quad (3)$$

The basis functions $\Psi_i(\boldsymbol{\xi})$ in (3) are generated from

$$\Psi_i(\boldsymbol{\xi}) = \prod_{k=1}^d \Psi_{i_k}(\xi_k), \quad i \in \mathcal{I}_{d,p}, \quad (4)$$

where $\Psi_{i_k}(\xi_k)$ are univariate polynomials of degree $i_k \in \mathbb{N}_0 := \mathbb{N} \cup \{0\}$, orthogonal with respect to $\rho(\xi_k)$ (see, e.g., Table A.7), i.e.,

$$\mathbb{E}[\Psi_{i_k} \Psi_{j_k}] = \langle \Psi_{i_k} \Psi_{j_k} \rangle = \int \Psi_{i_k}(\xi_k) \Psi_{j_k}(\xi_k) \rho(\xi_k) d\xi_k = \delta_{i_k j_k} \mathbb{E}[\Psi_{i_k}^2]. \quad (5)$$

Here $\delta_{i_k j_k}$ denotes the Kronecker delta and $\mathbb{E}[\cdot]$ is the expectation operator.

The number P of PC basis functions of total order $P < p$ in dimension d can be calculated to

$$P = |\mathcal{I}_{d,p}| = \frac{(p+d)!}{p!d!}.$$

The PC basis functions $\Psi_i(\boldsymbol{\xi})$ are orthogonal,

$$\mathbb{E}[\Psi_i \Psi_j] = \delta_{i,j} \mathbb{E}[\Psi_i^2], \quad (6)$$

because of the orthogonality of $\Psi_{i_k}(\xi_k)$ and the independence of ξ_k . As $p \rightarrow \infty$, the truncated PC expansion in (3) converges in the mean-square sense, iff the following two conditions are fulfilled: 1) $u(\boldsymbol{\xi})$ has finite variance and 2) the coefficients α_i are computed from the projection equation [20]

$$\alpha_i = \mathbb{E}[u(\cdot) \Psi_i(\cdot)] / \mathbb{E}[\Psi_i^2]. \quad (7)$$

2.3. Non-intrusive polynomial chaos expansion

In PC-based methods, one obtains the coefficients of the solution expansion either intrusively [29] or non-intrusively [30]. An intrusive approach

requires significant modification of the deterministic solvers, which increases the number of equations by a factor P . As a consequence the intrusive PC expansion method is P times more computationally expensive than a corresponding non-intrusive model.

Non-intrusive methods on the other hand can make use of existing deterministic solvers (\mathcal{M}) as black boxes. First, one needs to generate a set of N deterministic or random samples of ξ , denoted by $\{\xi^{(i)}\}_{i=1}^N$. The second step is to generate N realisations of the output QoI, $\{u(\xi^{(i)})\}_{i=1}^N$, with the available deterministic solver \mathcal{M} and without any solver modifications. The third and final step is to solve for the PC coefficients using the obtained realisations. Methods such as least squares regression [31], pseudo-spectral collocation [17], Monte Carlo sampling [32], and compressive sampling [33] are available. Along these lines an in depth discussion on least squares regression and compressive sampling can be found in [14, 3.1.1, 3.1.2].

The mean, $\mathbb{E}[\cdot]$, and variance, $\text{Var}[\cdot]$, of $u(\xi)$ can be directly approximated from the PC coefficients because of polynomial basis orthogonality given by

$$\mathbb{E}[\hat{u}] = \alpha_0, \quad (8)$$

and

$$\text{Var}[\hat{u}] = \sum_{\substack{i \in \mathcal{I}_{d,p} \\ i \neq 0}} \alpha_i^2 \mathbb{E}[\Psi^2(\xi_i)]. \quad (9)$$

A more complete description will be shown later in Section 2.5.

2.4. Global sensitivity analysis

The expensive, deterministic high fidelity particle accelerator model, \mathcal{M} , is described by a function $\mathbf{u} = \mathcal{M}(\mathbf{x})$, where the input \mathbf{x} is a point inside \mathcal{D} (c.f. Figure 1) and \mathbf{u} is a vector of QoI's. Finding correlations in these high dimensional spaces is nontrivial, however it is vital for a deep understanding of the underlying physics. For example, reducing the search space is of great interest in the modelling and optimisation process. In the spirit of Sobol' [34], let $\mathbf{u}^* = \mathcal{M}(\mathbf{x}^*)$ be the sought (true) solution. The local sensitivity of the solution \mathbf{u}^* with respect to x_k is estimated by $(\partial \mathbf{u} / \partial x_k)_{\mathbf{x}=\mathbf{x}^*}$. On the contrary, the global sensitivity approach does not specify the input $\mathbf{x} = \mathbf{u}^*$, it only considers the model $\mathcal{M}(\mathbf{x})$. Therefore, global sensitivity analysis should be regarded as a tool for studying the mathematical model rather than a specific solution ($\mathbf{x} = \mathbf{x}^*$).

Following [34], the problems that can be studied, in our context, with global sensitivity analysis can be categorised the following way:

1. ranking of variables in $\mathbf{u} = \mathcal{M}(x_1, x_2, \dots, x_n)$
2. identifying variables with low impact on \mathbf{u} .

In this article, we use the Sobol' indices [34] which are widely used due to their generality. Results can be found in Section 4.5.

The first order PC-based Sobol' index, S_k , represents the individual effects of the random input ξ_k on the variability of $u(\boldsymbol{\xi})$, and is given by

$$S_k = \frac{1}{\text{Var}[u(\boldsymbol{\xi})]} \sum_{\mathbf{i} \in \mathcal{I}_k} \alpha_{\mathbf{i}}^2 \mathbb{E}[\Psi^2(\xi_{\mathbf{i}})], \quad \mathcal{I}_k = \{\mathbf{i} \in \mathbb{N}_0^d : i_k > 0, i_{m \neq k} = 0\}. \quad (10)$$

In order to compute S_k , all random inputs except ξ_k are fixed. As a consequence, S_k does not include effects arising from the interactions between ξ_k and the other random inputs. This also means that \mathcal{I}_k includes only the dimension k .

The fractional contribution to the total variability of $u(\boldsymbol{\xi})$ due to parameter ξ_k , considering all other model parameters, is given by

$$S_k^T = \frac{1}{\text{Var}[u(\boldsymbol{\xi})]} \sum_{\mathbf{i} \in \mathcal{I}_k^T} \alpha_{\mathbf{i}}^2 \mathbb{E}[\Psi^2(\xi_{\mathbf{i}})] \quad \mathcal{I}_k^T = \{\mathbf{i} \in \mathbb{N}_0^d : i_k > 0\}. \quad (11)$$

The set of multi indices \mathcal{I}_k^T includes dimension k among others.

Now we are in a position to rank the importance of the variables. The smaller S_k^T is, the less important the random input, ξ_k , becomes. We note, for the extreme case $S_k^T \ll 1$, the variable ξ_k is considered to be insignificant. In such a case, the variable can be replaced by its mean value without considerable effects on the variability of $u(\boldsymbol{\xi})$. We will make use of this fact when discussing the model problem and use S_k^T as a measure to identify the most important random inputs of the model.

If one is interested in the fraction of the variance that is due to the joint contribution of the i -th and j -th input parameter, we can easily compute

$$S_{i,j} = \frac{1}{\text{Var}[u(\boldsymbol{\xi})]} \sum_{\mathbf{i} \in \mathcal{I}_{i,j}} \alpha_{\mathbf{i}}^2 \mathbb{E}[\Psi^2(\xi_{\mathbf{i}})] \quad \mathcal{I}_{i,j} = \{\mathbf{i} \in \mathbb{N}_0^d : i_k > 0\}. \quad (12)$$

which describes this quantity.

As an example to category 1 from above, consider a problem where x_i and x_j are two entries in the matrix of the second order moments of the initial particle distribution within a simulation. We then find out that S_i and S_j are both much smaller than $S_{i,j}$. Such a situation will indicate that other entries in the matrix of second order moments significantly contribute. For category 2, refer to [34, Section 7.], where an approximation of S is proven, when not considering all elements of x .

2.5. The UQTk based framework

In this section a detailed description is provided on how the particle accelerator UQ framework is constructed. The framework is based on the Uncertainty Quantification Toolkit (UQTk) [35], a lightweight C++/Python library that helps performing basic UQ tasks including intrusive and non-intrusive forward propagation. UQTk can also be used for inverse modelling via Bayesian or optimisation techniques. The corresponding tools used from UQTk are indicated in typewriter style in the following algorithm.

Let's denote \mathcal{M} as the black box solver, λ as the model parameters and y as the design or controllable parameter, with l equidistant values¹. The nonintrusive propagation of uncertainty from the d -dimensional model parameter λ to the output $u_i = \mathcal{M}(\lambda, y_i)$ follows a collocation procedure, given a d -dimensional basis $\Psi = (\Psi_1, \dots, \Psi_d)$ and $K = \frac{(d+p)!}{d!p!}$ multivariate basis terms with p being the maximal polynomial order.

Algorithm: generate for each y_i (design or controllable), a PC surrogate model

1. generate $N = (p + 1)^d$ quadrature point-weight pairs (ξ^n, w_n) (generate_quad)
2. for each of quadrature point ξ^n compute corresponding model input λ^n by

$$\lambda^n = \lambda_j^n = \sum_{k=0}^{K-1} \lambda_{jk} \Psi_k(\xi^n) \quad j = 1, \dots, d. \quad (13)$$

¹For a fixed value of the design parameter, the surrogate construction algorithm is described in [11].

3. create the training points with high fidelity simulations (OPAL)

$$u_i^n = \mathcal{M}(\boldsymbol{\lambda}^n, y_i) \quad i = 1, \dots, l. \quad (14)$$

4. calculate the expectation via orthogonal projection (`pce_resp`) using quadrature

$$\alpha_{ki} = \frac{\langle u \Psi_k \rangle}{\langle \Psi_k^2 \rangle} = \frac{1}{\langle \Psi_k^2 \rangle} \sum_{n=1}^N u_i^n \Psi_k(\boldsymbol{\xi}^n) w_n, \quad k = 0, \dots, K-1. \quad (15)$$

5. Given the computed α_{ki} values for each i and k , one assembles the PCE

$$\hat{u}_i = \sum_{k=0}^{K-1} \alpha_{ki} \Psi_k(\boldsymbol{\xi}), \quad k = 0, \dots, K-1. \quad (16)$$

Remark 1: The input PC in Eq. (13) is assumed to be given by an expert. For example, often only bounds for the inputs are known, in which case, Eq. (13) is simply a linear PC or just scaling from $\xi_j \in [-1, 1]$ to $\lambda_j \in [a_j, b_j]$ for each $j = 1, \dots, d$. More explicitly stated, in Eq. (13) $\lambda_{j0} = \frac{a_j + b_j}{2}$, and $\lambda_{jk} = \delta_{jk} \frac{b_j - a_j}{2}$. Thus, Eq. (13) becomes

$$\lambda_j^n = \frac{b_j + a_j}{2} + \frac{b_j - a_j}{2} \xi_j^n. \quad (17)$$

Remark 2: If samples $\boldsymbol{\xi}^n$ are randomly selected from the distribution of $\boldsymbol{\xi}$, then the projection formula (15) still holds, as long as one sets $w_n = 1/N$ for all n , and it becomes an importance sampling Monte-Carlo.

2.5.1. Evaluation of the Surrogate model

Having constructed the PC-coefficients, according to (15) the utility `pce_eval` can be used to evaluate \hat{u}_i (16).

2.5.2. Sensitivity Analysis

As shown in Section 2.4, the same information used in the surrogate model construction can be used in the sensitivity analysis. In the UQTK `pce_sens` will compute the total and joint sensitivities along with the variance fraction of each PC term individually.

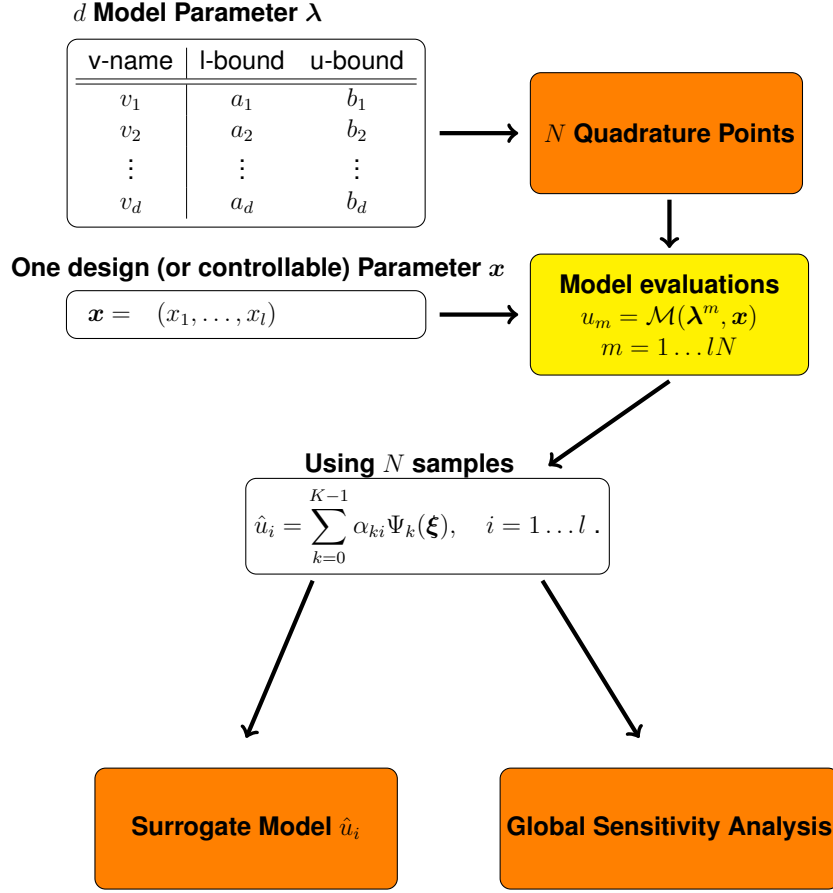


Figure 2: Uncertainty Quantification Framework

3. THE ACCELERATOR SIMULATION MODEL

For this discussion we briefly introduce OPAL-CYCL [36], one of the four flavours of OPAL. OPAL will be used as the back-box solver denoted by \mathcal{M} in (14).

3.1. Governing Equation

In the cyclotron under consideration, the collision between particles can be neglected because the typical bunch density is low. In time domain, the general equations of motion for charged particles in electromagnetic fields

can be expressed by

$$\frac{d\mathbf{p}(t)}{dt} = q (c\boldsymbol{\beta} \times \mathbf{B} + \mathbf{E}),$$

where m_0, q, γ are the rest mass, the charge and the relativistic factor. Here we denote $\mathbf{p} = m_0 c \gamma \boldsymbol{\beta}$ as the momentum of a particle, c as the speed of light, and $\boldsymbol{\beta} = (\beta_x, \beta_y, \beta_z)$ as the normalised velocity vector. In general, the time (t) and the position (\mathbf{x}) dependent electric and magnetic vector fields are written in an abbreviated form as \mathbf{B} and \mathbf{E} .

If \mathbf{p} is normalized by $m_0 c$, Eq. (18) can be written in Cartesian coordinates as

$$\begin{aligned} \frac{dp_x}{dt} &= \frac{q}{m_0 c} E_x + \frac{q}{\gamma m_0} (p_y B_z - p_z B_y), \\ \frac{dp_y}{dt} &= \frac{q}{m_0 c} E_y + \frac{q}{\gamma m_0} (p_z B_x - p_x B_z), \\ \frac{dp_z}{dt} &= \frac{q}{m_0 c} E_z + \frac{q}{\gamma m_0} (p_x B_y - p_y B_x). \end{aligned} \quad (18)$$

The evolution of the beam's distribution function, $f(\mathbf{x}, c\boldsymbol{\beta}, t) : (\mathbb{R}^M \times \mathbb{R}^M \times \mathbb{R}) \rightarrow \mathbb{R}$, can be expressed by a collisionless Vlasov equation:

$$\frac{df}{dt} = \partial_t f + c\boldsymbol{\beta} \cdot \nabla_{\mathbf{x}} f + q(\mathbf{E} + c\boldsymbol{\beta} \times \mathbf{B}) \cdot \nabla_{c\boldsymbol{\beta}} f = 0. \quad (19)$$

Here it is assumed that M particles are within the beam. In this particular case, \mathbf{E} and \mathbf{B} include both externally applied fields and space charge fields.

$$\begin{aligned} \mathbf{E} &= \mathbf{E}_{\text{ext}} + \mathbf{E}_{\text{sc}}, \\ \mathbf{B} &= \mathbf{B}_{\text{ext}} + \mathbf{B}_{\text{sc}}. \end{aligned} \quad (20)$$

All other fields are neglected.

3.2. Self Fields

The space charge fields can be obtained by a quasi-static approximation. In this approach, the relative motion of the particles is non-relativistic in the beam rest frame, thus the self-induced magnetic field is practically

absent and the electric field can be computed by solving Poisson's equation

$$\nabla^2 \phi(\mathbf{x}) = -\frac{\rho(\mathbf{x})}{\varepsilon_0}, \quad (21)$$

where ϕ and ρ are the electrostatic potential and the spatial charge density in the beam rest frame. The electric field can then be calculated by

$$\mathbf{E}_{\text{sc}} = -\nabla \phi, \quad (22)$$

and back transformed to yield both the electric and the magnetic fields, in the lab frame, as required in Eq. (20) by means of a Lorentz transformation. Because of the large vertical gap in our cyclotron, the contributions from image charges and currents are minor compared to space charge effects [37], and hence it is a good approximation to use open boundary conditions. Details on the space charge calculation methods utilised in OPAL can be found in [36, 38, 39]

3.3. External Fields

With respect to the external magnetic field, two possible situations can be considered. In the first situation, the real field map is available on the median plane of the existing cyclotron machine using measurement equipment.

In most cases concerning cyclotrons, the vertical field, B_z , is measured on the median plane ($z = 0$) only. Since the magnetic field outside the median plane is required to compute trajectories with $z \neq 0$, the field needs to be expanded in the Z direction.

According to the approach given by Gordon and Taivassalo [40], by using a magnetic potential and measured B_z on the median plane at the point (r, θ, z) in cylindrical polar coordinates, the 3rd order field can be written as

$$\mathbf{B}_{\text{ext}}(r, \theta, z) = \left(z \frac{\partial B_z}{\partial r} - \frac{1}{6} z^3 C_r, \frac{z}{r} \frac{\partial B_z}{\partial \theta} - \frac{1}{6} \frac{z^3}{r} C_\theta, B_z - \frac{1}{2} z^2 C_z \right), \quad (23)$$

where $B_z \equiv B_z(r, \theta, 0)$ and

$$\begin{aligned} C_r &= \frac{\partial^3 B_z}{\partial r^3} + \frac{1}{r} \frac{\partial^2 B_z}{\partial r^2} - \frac{1}{r^2} \frac{\partial B_z}{\partial r} + \frac{1}{r^2} \frac{\partial^3 B_z}{\partial r \partial \theta^2} - 2 \frac{1}{r^3} \frac{\partial^2 B_z}{\partial \theta^2}, \\ C_\theta &= \frac{1}{r} \frac{\partial^2 B_z}{\partial r \partial \theta} + \frac{\partial^3 B_z}{\partial r^2 \partial \theta} + \frac{1}{r^2} \frac{\partial^3 B_z}{\partial \theta^3}, \\ C_z &= \frac{1}{r} \frac{\partial B_z}{\partial r} + \frac{\partial^2 B_z}{\partial r^2} + \frac{1}{r^2} \frac{\partial^2 B_z}{\partial \theta^2}. \end{aligned} \quad (24)$$

All the partial differential coefficients are computed on the median plane data by interpolation, using Lagrange's 5-point formula.

In the second situation, a 3D field map for the region of interest is calculated numerically from a 3D model of the cyclotron. This is generally performed during the design phase of the cyclotron and utilises commercial software. In this case the calculated field will be more accurate, especially at large distances from the median plane, i.e. a full 3D field map can be calculated. For all calculations in this paper, we use the Gordon and Taivassalo [40] method.

For the radio frequency cavities, a radial voltage profile $V(r)$ along the radius of the cavity is used. The gap-width, g , is included in order to correct for the transit time. For the time dependent field,

$$\Delta E_{\text{rf}} = \frac{\sin \tau}{\tau} \Delta V(r) \cos(\omega_{\text{rf}} t - \phi), \quad (25)$$

with F denoting the transit time factor ($F = \frac{1}{2} \omega_{\text{rf}} \Delta t$), and Δt the transit time defined by

$$\Delta t = \frac{g}{\beta c}. \quad (26)$$

In addition, a voltage profile varying along radius will give a phase compression of the bunch, which is induced by an additional magnetic field component B_z in the gap,

$$B_z \simeq \frac{1}{g \omega_{\text{rf}}} \frac{dV(r)}{dr} \sin(\omega_{\text{rf}} t - \phi). \quad (27)$$

From (27) we can calculate a horizontal deflection, α , as

$$\alpha \simeq \frac{q}{m_0 \beta \gamma c \omega_{\text{rf}} t} \frac{dV(r)}{dr} \sin(\omega_{\text{rf}} t - \phi). \quad (28)$$

Finally, in this paper, both the external fields and space charge fields are used to track particles for one time step using a 4th order Runge-Kutta (RK) integrator. This means the fields are evaluated for four times in each time step. Space charge fields are assumed to be constant during one time step because their variation is typically much slower than that of external fields.

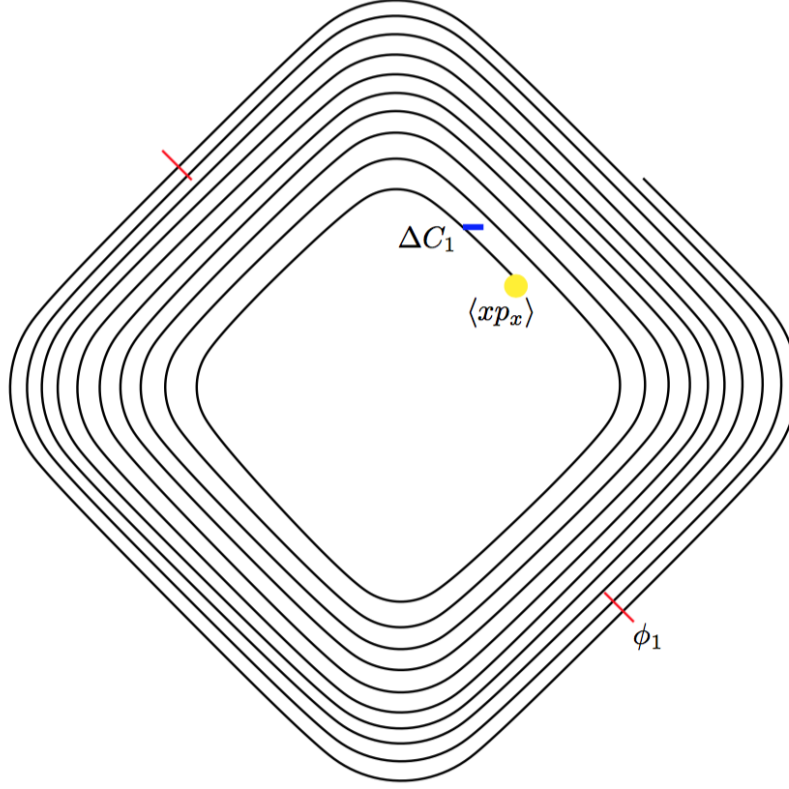


Figure 3: The cyclotron model problem setup. The two red lines indicating the 2 double gap flat-top resonators, the blue line represents a collimator, and the yellow circle stands for the initial conditions.

4. APPLICATION OF THE UQ FRAMEWORK

In order to demonstrate the usefulness and strength of UQ, consider a simplified model of the PSI Injector 2 cyclotron which is sketched in Figure 3. The simplifications are as follows: 1) only energies up to 8.5 MeV (turn 10) are considered to reduce the computational burden. 2) a Gaussian distribution, linearly matched to the injection energy of 870 keV, is used for the initial conditions. 3) the magnetic field and RF structures are the same as in our full production simulation. 4) P_r and R are obtained from equilibrium orbit simulations, and 5) one collimator is introduced in order to mimic bunch shaping. Full scale high fidelity simulations of this kind can be found in [41, 42], where similar physics goals have been pursued.

4.1. Model parameters

In typical design studies of high power cyclotrons, the high number of model parameters are such that one can not fully scan their entire range. For this feasibility study, one model parameter out of a family of three important categories (c.f. Figure 3) was chosen:

1. initial conditions: model parameter $\langle xp_x \rangle$, correlation between initial the x and p_x phase space variables
2. collimator settings: model parameter ΔC_1 position of the collimator
3. rf phase settings: model parameter ϕ_1 defines the phase of the acceleration cavity.

From previous experience, these three categories have the most influence when designing and optimising high precision models of high power cyclotrons. The relationship of the parameters with uncertainties, $\lambda_1, \lambda_2, \lambda_3$, is shown in Figure 2.

4.2. Quantities of interest (QoI)

The phase space spanned by M macro particles, in the high fidelity OPAL model (simulation), is given by $(\mathbf{q}_i(t), \mathbf{p}_i(t)) \in \Gamma \subset \mathbb{R}^{(2M+1)}$ and $i = x, y, z$. We identify a subset of interesting QoI's such as:

1. $\tilde{\epsilon}_x = \sqrt{\langle \mathbf{q}_x^2 \mathbf{p}_x^2 \rangle - \langle \mathbf{q}_x \mathbf{p}_x \rangle^2}$ the rms projected emittance and \tilde{x} the rms beam size,
2. the kinetic energy E and rms energy spread ΔE ,
3. $h_t = \frac{\langle \mathbf{q}_x^4 \rangle}{\langle \mathbf{q}_x^2 \rangle^2} - c$, the halo parameter in x -direction at end of turn t with $c \in \mathbb{R}$, a distribution dependent normalisation constant.

The rms beam size \tilde{x} is one of the better quantities that can be directly measured and hence among the first candidate for characterisation of the particle beam. A measure of the projected phase space volume is the emittance $\tilde{\epsilon}_x$. This quantity is often used for the estimation of the beam quality. The two energy related parameters E and ΔE are target values to achieve, the first one closely related to the experiment where the particle beam is designed for, the energy spread ΔE is directly related to the beam quality in the case of the presented model problem. Minimizing the halo of the particle beam is equal to minimizing losses, the most important quantity to optimize in high power hadron accelerators. In the formulation of h_t , this parameter is deviating from 1 iff the initial chooses distribution

is changing. If the initial distribution is a stationary distribution, this measure can be attributed to the mechanism of halo generation, in case of a deviation from the value 1.

In the case of a high intensity cyclotron model, we choose the controllable parameter y as the average current.

4.3. UQ model setup

The controllable parameters are not modelled with polynomials, but rather given by 10 equidistant values from 1...10 mA. As a next step, the polynomial type for the model parameter is chosen according to the Wiener-Askey scheme (cf. Appendix Appendix A). The distribution of the three model parameters $\langle xp_x \rangle$, ΔC_1 , and the phase ϕ_1 , are modelled according to an uniform distribution using polynomials of the Legendre type. The bounds of the distribution are given in Table 1. Other parameters for

Table 1: Upper and lower bounds of the design parameters

v-name	l-bound	u-bound
$\langle xp_x \rangle$	-0.5	0.5
ΔC_1 (mm)	0	5
ϕ_1 (°)	-20	20

the UQ model are listed in Table 5.

Table 2: Summary of UQ related parameters for the presented results. The dimension for all the experiments are $d = 3$. The one controllable parameter y has length $l = 10$.

Parameter	Meaning	Experiment	3	2	1
p	order of surrogate construction		2	3	4
	quadrature points per dimension $(p + 1)$		3	4	5
N	quadrature points $N = (p + 1)^d$		27	64	125
K	polynomial basis terms $K = (d + p)!/d!p!$		10	20	35
$N \cdot l$	number of high-fidelity runs		270	640	1250

4.4. High Fidelity Simulations vs. Surrogate Model

As a first method to determine the validity of the surrogate model, the values of the high fidelity OPAL simulations on the x-axis and the values of the surrogate model on the y-axis were compared. The distance of the corresponding point to the line $x = y$, is a measure of surrogate model's quality. The QoI's, as defined in Section 4.2, are compared for a subset of controllable parameters: 1, 5, 8, and 10 mA, and for 3 different orders of the surrogate model, as described in Table 5. All data from the surrogate model and the high fidelity model are taken at the end of turn 10 in our model problem.

Overall the expected convergence is observed when increasing p as shown in Figure 4 through Figure 9, and furthermore this is supported by the L_2 error norm shown in Section 4.6.

4.4.1. Projected Emittance & Beam size

Given the fact that the emittance is a very sensitive quantity, measuring phase space volume, it is surprising, but also promising, that such a good agreement between the surrogate model and the high fidelity model can be achieved. This is graphically illustrated in Figure 4 and Figure 5. The maximum error in % is given in Table 3 and Table 4, and is below 7% for all considered cases.

Table 3: Maximum error in % between the high fidelity and surrogate model for the projected emittance $\tilde{\varepsilon}_x$ of the beam.

	$P = 4$	$P = 3$	$P = 2$
$I = 1$ (mA)	1.94	2.81	3.35
$I = 5$ (mA)	5.04	4.77	2.79
$I = 8$ (mA)	4.89	4.95	6.70
$I = 10$ (mA)	3.6	2.78	5.60

Table 4: Maximum error in % between the high fidelity and surrogate model for the rms beam size \tilde{x} of the beam.

	$P = 4$	$P = 3$	$P = 2$
$I = 1$ (mA)	0.70	0.87	1.03
$I = 5$ (mA)	2.32	2.90	3.49
$I = 8$ (mA)	1.04	3.33	1.86
$I = 10$ (mA)	1.33	1.98	1.39

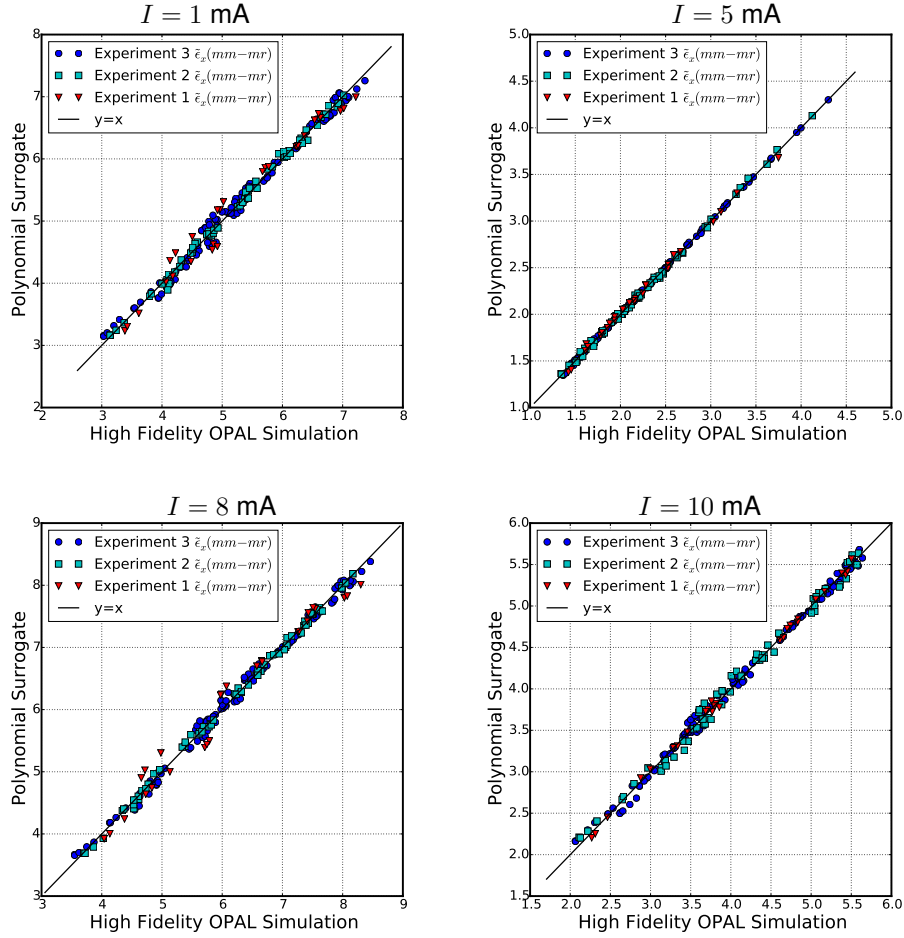


Figure 4: Projected emittance $\tilde{\epsilon}_x$ (mm-mr) for all 3 experiments described in Table 5.

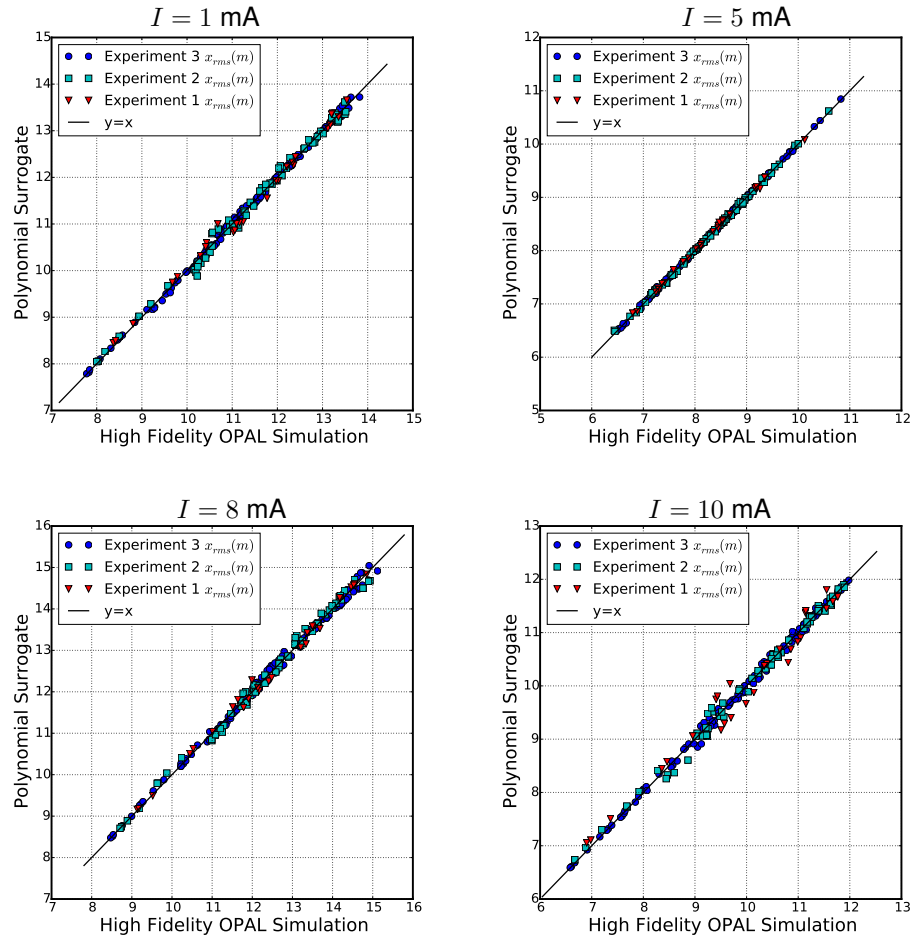


Figure 5: RMS beam size \tilde{x} (mm) for all 3 experiments described in Table 5.

4.4.2. Final Energy

The energy dependence shown in Figure 6 for 10 mA, illustrated the same expected behaviour for all other intensities. This is because of the small gain the third harmonic cavity is suppose to deliver (in the PSI Injector 2 we use the third harmonic cavity for acceleration). For the given experiment only the last two turns are contributing. This fact is even better illustrated, when looking at the maximum error which is $\leq 0.07\%$, as seen in Table 5.

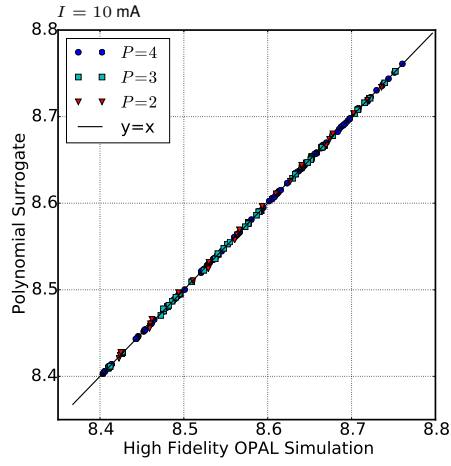


Figure 6: Final Energy E (MeV) for $I = 10$ mA, and all experiments described in Table 5.

Table 5: Maximum error in % between the high fidelity and surrogate model for the final energy of the beam.

	$P = 4$	$P = 3$	$P = 2$
$I = 1$ (mA)	0.013	0.017	0.070
$I = 5$ (mA)	0.013	0.036	0.066
$I = 8$ (mA)	0.014	0.029	0.057
$I = 10$ (mA)	0.010	0.027	0.056

4.4.3. RMS Energy Spread

Despite the fact the rms energy spread is influenced by space charge, the collimation, and the change in phase, a very good agreement with absolute deviations $\leq 5\%$ were obtained. Table 6 shows details.

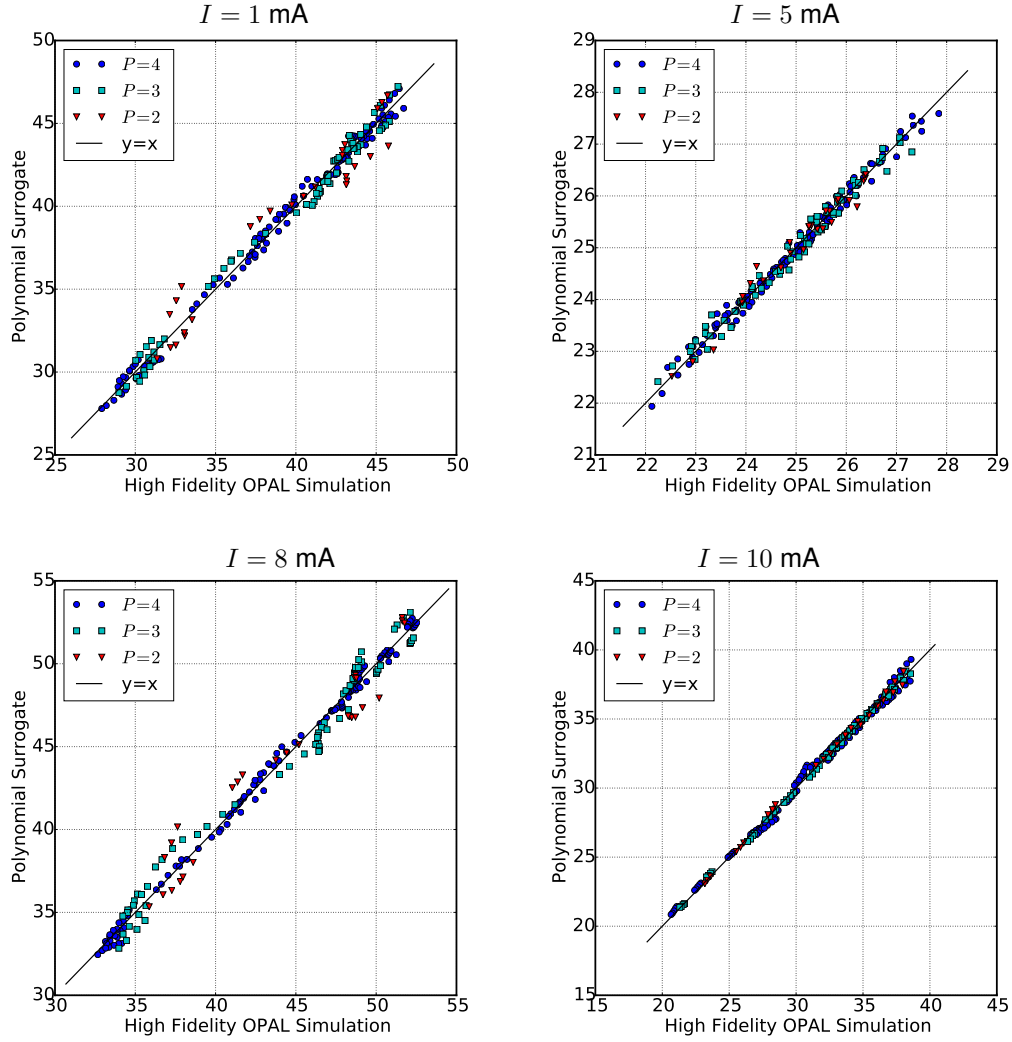


Figure 7: Energy spread ΔE (keV) for all 3 experiments described in Table 5.

Table 6: Maximum error in % between the high fidelity and surrogate model for the energy spread ΔE of the beam.

	$P = 4$	$P = 3$	$P = 2$
$I = 1$ (mA)	0.97	1.67	1.62
$I = 5$ (mA)	2.56	1.04	1.29
$I = 8$ (mA)	2.56	2.75	4.65
$I = 10$ (mA)	3.00	3.70	4.48

4.4.4. Halo Parameters

The halo parameter was evaluated at turn 5 (Figure 8) and at turn 10 (Figure 9). As anticipated the halo grows and the surrogate model has a maximum absolute error of $\leq 5\%$, again a very good accuracy.

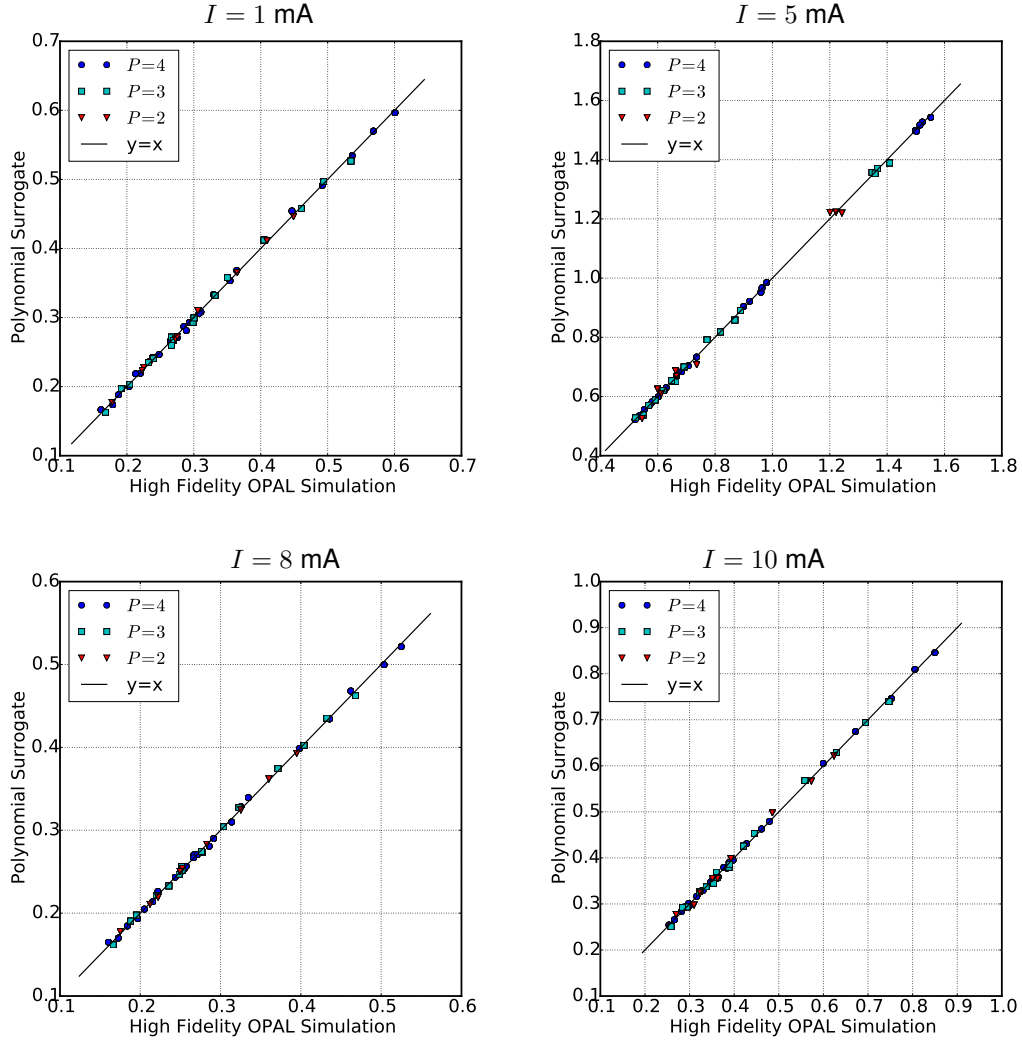


Figure 8: The dimensionless halo parameter h after turn 5 for all 3 experiments described in Table 5.

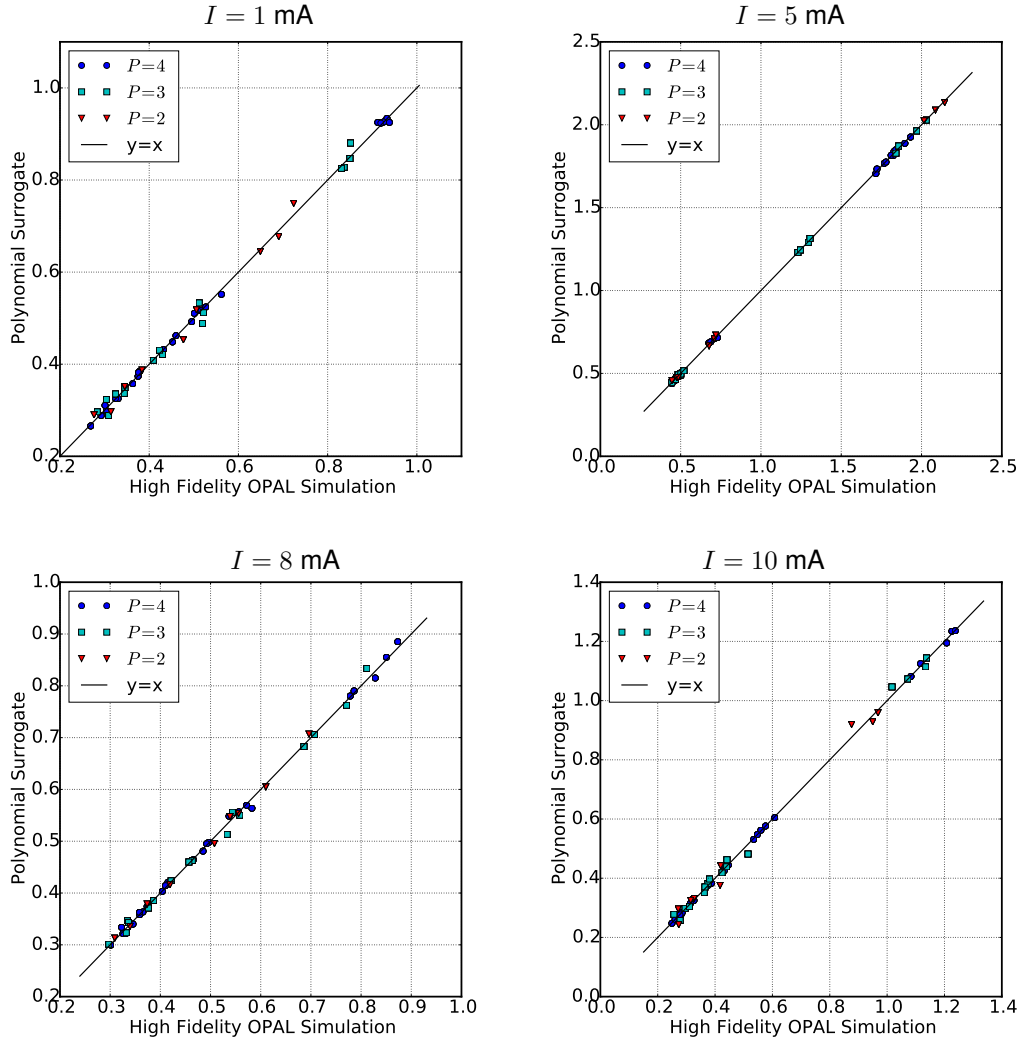


Figure 9: The dimensionless halo parameter h after turn 10 for all 3 experiments described in Table 5.

4.5. Sensitivity Analysis

S_k in (10) can be interpreted as the fraction of the variance in model \mathcal{M} that can be attributed to the i -th input parameter only. S_k^T in (11) measures the fractional contribution to the total variance due to the i -th parameter and its interactions with all other model parameters. In the sequel an analysis based of S_k^T is shown for the model problem.

Figure 10 showing, for a subset of the controllable parameter I , sensitivities of the QoI's with respect to the model parameters. The polynomial order is $P = 4$, the similar correlations for other orders are not shown. Correlations, for example the insensitivity of the energy, and x , p_x or the

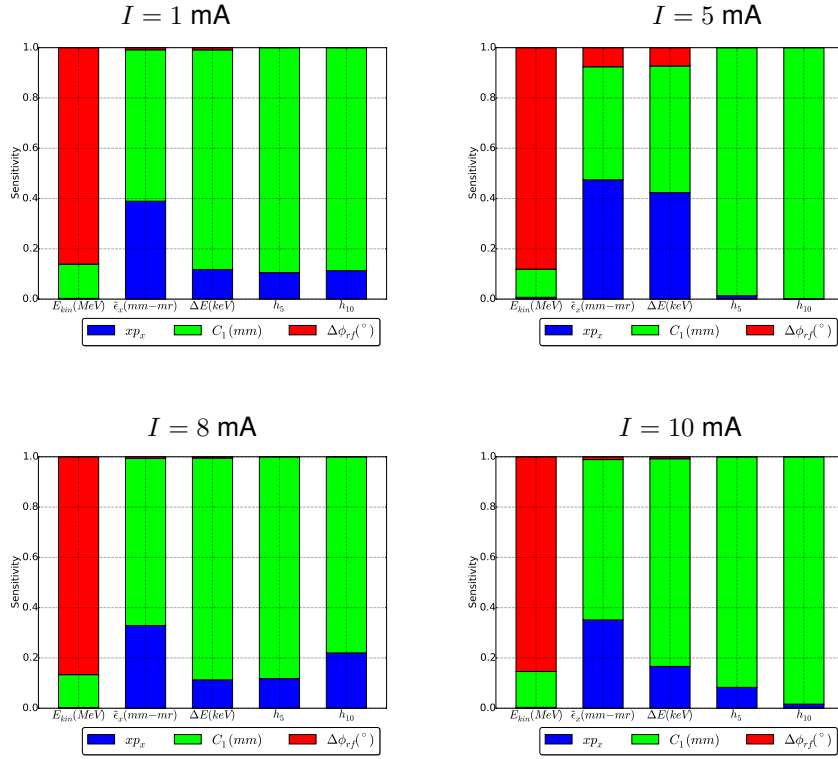


Figure 10: Experiment 1: Global sensitivity analysis for intensities of 1,5,8 and 10 mA

significant energy phase correlation, are consistent with what is anticipated. A very mild dependency on x , p_x is observed and expected. There is a phase correlation appearing in the case of $I = 5$ mA, which seems

to be suppressed at other intensities, and the initial correlation of the distribution seems to become insignificant. A closer inspection of the phase space, beyond the scope of that paper, hints that the halo at this intensity has a minimum. This could explain the observed behaviour and is subject to a deeper investigation.

These are very interesting findings that can guide new designs but also improve existing accelerators, and shows quintessential the merit and power of such a sensitivity analysis.

4.6. Error Propagation and L_2 Error

In Figure 11, the L_2 error

$$L_2 = \frac{||\hat{u} - u||_2}{||\hat{u}||_2}$$

between the surrogate model \hat{u} and u , the high fidelity OPAL model, is shown for E , the final energy of the particle beam and all values of the controllable parameter I . The mean value and variance are shown on the left y-axis. We can now precisely define the error and the dependency of the surrogate model on P . The expected convergence of the surrogate model as function of P is shown for one model parameter only, because of the similar behaviour in the other considered parameters. This clearly help in choosing an appropriate order of the surrogate model.

4.7. Extrapolation

The surrogate model is constructed by selecting an appropriate number of training points in order to sample the input uncertainties of the design parameter space. These finite number of training points are depicted as yellow points in Figure 12. However, with the surrogate model we can choose any point within the lower and upper bound specified (a_i, b_i in (17)) in order to obtain λ in (13). This we call extrapolation. In Figure 12 the red points are arbitrarily chosen, within the specified bounds and they are very we within the bounds of the surrogate model and the 95% confidence level (CL) obtained by evaluating the Student-t test.

4.8. Performance

The presented surrogate model is the most simple, but gives for the non trivial model problem, statistically sound results. This fact and the remark

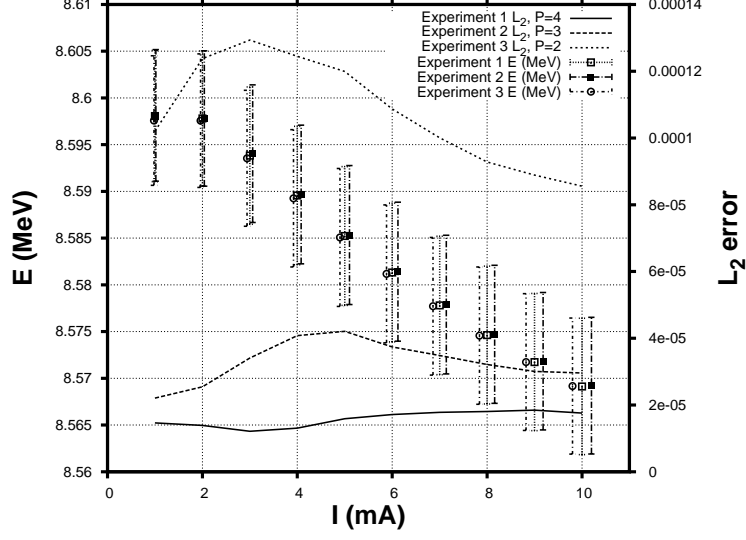


Figure 11: Medium values, and variances are shown on the left y-axis for the extraction energy E . The global L_2 error between the high fidelity and the surrogate model, for the final energy of the particle beam, is shown on the right y-axis.

that the evaluation of the surrogate model is $\sim 800\times$ faster than the high fidelity model (400 seconds v.s. 0.5 seconds) opens up unprecedented possibilities in research areas such as on-line modelling and multi-objective [43, 44] optimization of charged particle accelerators.

5. CONCLUSIONS

A sampling-based UQ approach is presented to study, for the first time, the effects of input uncertainties on the performance of particle accelerators. A particular, but complex, example in the form of a high intensity cyclotron was used to demonstrate the usefulness of the surrogate model as well as the global sensitivity analysis via computing the total Sobol' indices. The presented physics problem is a model problem, with the aim of demonstrating the usefulness and applicability of the presented UQ ap-

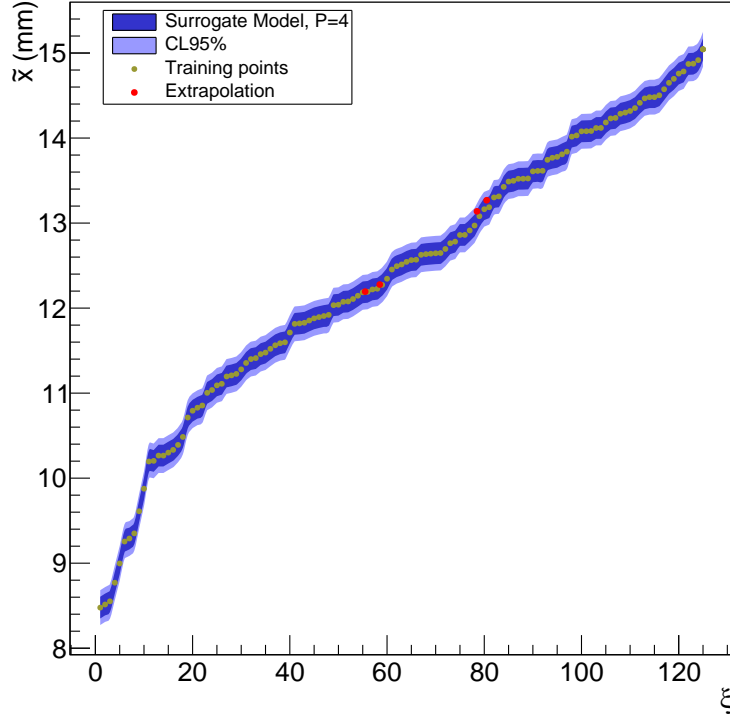


Figure 12: The surrogate mode for \tilde{x} , together with training and extrapolation points. The 95% CL of the model is also shown.

proach. However, we claim to present a problem that can be recognised as a template for many high intensity modelling attempts, and beyond.

The proposed UQ approach is based on polynomial chaos expansion using the UQTK software. The goal is to achieve an accurate estimation of solution statistics using a minimal number of high fidelity simulations. For several QoI's a surrogate model was constructed, the validity is proofed by comparing to a high fidelity model. L_2 error norms showing the expected convergence in regard to the degree of the polynomial chaos expansion. For the rms beam size (\tilde{x}), extrapolation points, i.e. points that are not used in the training set, where evaluated and compared to the statistical expectations from the model. We found that the values are consistent with

the surrogate model and very well within the 95% CL.

The Sobol' based global sensitivity analysis was in line with the expectation from the physics evaluation of the model problem.

A tremendous speedup of $800\times$ was observed, comparing the time to solution of the surrogate model to the high fidelity model. This opens up possibilities for on-line modelling and multi-objective optimization of complex particle accelerators.

Future research includes the application to real word problems in the area of high intensity hadron machines, i.e. performance enhancements of exiting machines and design improvements of future machines [41]. In the area of proton therapy, we focus on understanding the uncertainty of accelerator parameters, in relation to the applied radiation dose to the patient.

In this paper, conceptional we followed the simplest approach towards UQ. Given the encouraging results, we plan to enhance this model by using Hermite chaos, and going to higher dimensions, which implies the use of sparse methods or latin hyper cube sampling.

Particle accelerators in general create a vast amount of high quality data, including the QoI's we have considered. Including such data into the the model, or solving an inverse problem could be interesting research topics for the future.

6. ACKNOWLEDGMENTS

Dr. N. Pouge for critical comments and english proof reading. Ms. V. Rizzioglio for many fruitful discussion and help with the art work. Dr. K. Sargsyan & Dr. B. Debusschere for UQTk and UQ related discussions.

Appendix A. Wiener-Askey PC

Table A.7: The correspondence of Wiener-Askey PC and the pdf of the random variables [20].

$\rho(\xi_k)$	Polynomial	Support
Beta	Jacobi	[a,b]
Uniform	Legendre	[a,b]
Gaussian	Hermite	$(-\infty, +\infty)$
Gamma	Laguerre	$(0, +\infty)$

Appendix B. Legendre polynomials

The Legendre polynomials, or Legendre functions of the first kind (B.1), (Whittaker and Watson 1990, p. 302), are solutions to the Legendre differential equation, a second-order ordinary differential equation

$$(1 - x^2) \frac{d^2 y}{dx^2} - 2x \frac{dy}{dx} + l(l + 1)y = 0. \quad (\text{B.1})$$

In case of $l \in \mathcal{N}$, the solutions are polynomials P_n . The first few polynomials relevant to this paper are shown in (B.2).

$$\begin{aligned} P_0(x) &= 1 \\ P_1(x) &= x \\ P_2(x) &= 1/2(3x^2 - 1) \\ P_3(x) &= 1/2(5x^3 - 3x) \\ P_4(x) &= 1/8(35x^4 - 30x^2 + 3) \\ &\dots \end{aligned} \quad (\text{B.2})$$

References

References

- [1] R. E. Caflisch. Monte Carlo and quasi-Monte Carlo methods. *Acta Numerica*, 7:1–49, 1998.
- [2] H. Niederreiter. Quasi-Monte Carlo methods and pseudo-random numbers. *Bulletin of the American Mathematical Society*, 84(6):957–1041, 1978.
- [3] Stefan Pauli, Robert Nicholas Gantner, Peter Arbenz, and Andreas Adelmann. Multilevel monte carlo for the feynman-kac formula for the laplace equation. *BIT Numerical Mathematics*, 2015.
- [4] D. C. Montgomery R. H. Myers and C. M. Anderson-Cook. *Response Surface Methodology*. Wiley, third edition, 2009.
- [5] R. Tibshirani T. Hastie and J. Friedman. *The Elements of Statistical Learning*. Springer, second edition, 2009.

- [6] N. Wiener. The homogeneous chaos. *American Journal of Mathematics*, 60:897–936, 1938.
- [7] K. Sargsyan et al. Dimensionality reduction for complex models via bayesian compressive sensing. *International Journal of Uncertainty Quantification*, 4, 1:63–93, 2014.
- [8] R. Ghanem. Probabilistic characterization of transport in heterogeneous media. *Comput. Methods Appl. Mech. Engng.*, 158:199–220, 1998.
- [9] V. Fonoberov T. Sahai and S. Loire. Uncertainty as a stabilizer of the head-tail ordered phase in carbon-monoxide monolayers on graphite. *Physical Review B*, 80(11):115413, 2009.
- [10] H. N. Najm B. J. Debusschere Y. M. Marzouk S. Widmer and O. P. Le Maître. Uncertainty quantification in chemical systems. *Int. J. Numer. Meth. Engng.*, 80:789–814, 2009.
- [11] Habib N. Najm. Uncertainty Quantification and Polynomial Chaos Techniques in Computational Fluid Dynamics. *ANNUAL REVIEW OF FLUID MECHANICS*, 41:35–52, 2009.
- [12] D. Xiu and G. E. Karniadakis. Modeling uncertainty in flow simulations via generalized polynomialchaos. *J. Comp. Phys.*, 187:137–167, 2003.
- [13] B. Kouchmeshky and N. Zabaras. The effect of multiple sources of uncertainty on the convex hull of material properties of polycrystals. *Computational Materials Science*, 47(2):342–352, 2009.
- [14] Mohammad Hadigol, Kurt Maute, and Alireza Doostan. On uncertainty quantification of lithium-ion batteries: Application to an lic6/licoo2 cell. *Journal of Power Sources*, 300:507 – 524, 2015.
- [15] José Miguel Pasini and Tuhin Sahai. Polynomial chaos based uncertainty quantification in hamiltonian, multi-time scale, and chaotic systems. (2013). <http://arxiv.org/abs/1207.0016>.
- [16] Roger G. Ghanem and Pol D. Spanos. *Stochastic finite elements: a spectral approach*. Springer-Verlag, New York, 1991.

- [17] Dongbin Xiu. *Numerical methods for stochastic computations*. Princeton University Press, Princeton, NJ, 2010. A spectral method approach.
- [18] R. H. Cameron and W. T. Martin. The orthogonal development of non-linear functionals in series of Fourier-Hermite functionals. *Ann. of Math. (2)*, 48:385–392, 1947.
- [19] R.C. Smith. *Uncertainty Quantification*. SIAM, 2014.
- [20] Dongbin Xiu and George Em Karniadakis. The Wiener-Askey polynomial chaos for stochastic differential equations. *SIAM J. Sci. Comput.*, 24(2):619–644 (electronic), 2002.
- [21] Steven Strogatz. *Nonlinear dynamics and chaos: with applications to physics, biology, chemistry and engineering*. Perseus Books Group, 2001.
- [22] H. Ogura. Orthogonal functions of the Poisson processes. *IEEE Transactions on Information Theory*, 18(4):473–481, 1972.
- [23] X. Wan and G. E. Karniadakis. Beyond Wiener-Askey expansions: Handling arbitrary PDFs. *Journal of Scientific Computing*, 27:455–464, 2006.
- [24] Raul Tempone Fabio Nobile and Clayton G. Webster. A sparse grid stochastic collocation method for partial differential equations with random input data. *SIAM J. Numer. Anal.*, 46:2309–2345, 2008.
- [25] N. Zabaras and B. Ganapathysubramanian. A scalable framework for the solution of stochastic inverse problems using a sparse grid collocation approach. *J. Comput. Phys.*, 227:4697–4735, 2008.
- [26] Tuhin Sahai Amit Surana and Andrzej Banaszuk. Iterative methods for scalable uncertainty quantification in complex networks. *International Journal for Uncertainty Quantification*, 2(4):1–49, 2012.
- [27] Alberto Speranzon Tuhin Sahai and Andrzej Banaszuk. Hearing the clusters in a graph: A distributed algorithm. *Automatica*, 48:15–24, 2012.

- [28] Cong Liu Stefan Klus, Tuhin Sahai and Michael Dellnitz. An efficient algorithm for the parallel solution of high-dimensional differential equations. *J. Comput. Appl. Math.*, 235:3053–3062, 2011.
- [29] B. Debusschere et al. Numerical challenges in the use of polynomial chaos representations for stochastic processes. *SIAM Journal of Scientific Computing*, **26**:698–0719, 2004.
- [30] Michael S. Eldred. Recent advances in non-intrusive polynomial chaos and stochastic collocation methods for uncertainty analysis and design. In *50th AIAA/ASME/ASCE/AHS/ASC Structures, Structural Dynamics and Materials Conference*, 2009.
- [31] S. Hosder, R.W. Walters, and R. Perez. A non-intrusive polynomial chaos method for uncertainty propagation in CFD simulations. In *44th AIAA aerospace sciences meeting and exhibit AIAA-2006-891*, 2006.
- [32] O. P. Le Maître and O. M. Knio. *Spectral methods for uncertainty quantification*. Scientific Computation. Springer, New York, 2010. With applications to computational fluid dynamics.
- [33] Alireza Doostan and Houman Owhadi. A non-adapted sparse approximation of PDEs with stochastic inputs. *J. Comput. Phys.*, 230(8):3015–3034, 2011.
- [34] I.M. Sobol. Global sensitivity indices for nonlinear mathematical models and their monte carlo estimates. *Mathematics and Computers in Simulation*, 55(1-3):721–280, 2001.
- [35] Bert Debusschere, Khachik Sargsyan, and Cosmin Safta. UQTK Version 2.1. Technical Report SAND2014-4968, Sandia National Laboratories, 2014.
- [36] J. J. Yang, A. Adelmann, M. Humbel, M. Seidel, and T. J. Zhang. Beam dynamics in high intensity cyclotrons including neighboring bunch effects: Model, implementation, and application. *Phys. Rev. ST Accel. Beams*, 13(6):064201, Jun 2010.
- [37] R. Baartman. Intensity limitations in compact h- cyclotron. In *Proc. 14th Int. Conf. on Cyclotrons and their Applications*, page 440, Capetown, 1995.

- [38] A. Adelmann, P. Arbenz, and Y. Ineichen. A fast parallel Poisson solver on irregular domains applied to beam dynamics simulations. *J. Comp. Phys.*, 229(12):4554–4566, 2010.
- [39] R. W. Hockney and J. W. Eastwood. *Computer Simulation Using Particles*. Hilger, New York, 1988.
- [40] M. M. Gordon and V. Taivassalo. Nonlinear effects of focusing bars used in the extraction systems of superconducting cyclotrons. *IEEE Trans. Nucl. Sci.*, 32:2447, 1985.
- [41] J.J. Yang, A. Adelmann, W. Barletta, L. Calabretta, A. Calanna, D. Campo, and J.M. Conrad. Beam dynamics simulation for the high intensity cyclotrons. *Nuclear Instruments and Methods in Physics Research Section A: Accelerators, Spectrometers, Detectors and Associated Equipment*, 704:84 – 91, 2013.
- [42] YJ Bi, A Adelmann, R Dölling, M Humbel, W Joho, M Seidel, and TJ Zhang. Towards quantitative simulations of high power proton cyclotrons. *Physical Review Special Topics-Accelerators and Beams*, 14(5):054402, 2011.
- [43] Yves Ineichen, Andreas Adelmann, Costas Bekas, Alessandro Curi-
oni, and Peter Arbenz. A fast and scalable low dimensional solver for
charged particle dynamics in large particle accelerators. *Computer
Science - Research and Development*, pages 1–8, May 2012.
- [44] Y. Ineichen, A. Adelmann, A. Kolano, C. Bekas, A. Curioni, and
P. Arbenz. A parallel general purpose multi-objective optimiza-
tion framework, with application to beam dynamics. *arXiv preprint
arXiv:1302.2889*, 2013.